Research Article | Vol. 27, No. 22 / 28 October 2019 / Optics Express 31207
Optics EXPRESS

Extrinsic photoluminescence properties of individual micro-particle of Cs_4PbBr_6 perovskite with "defect" structure

LIULI YANG,[1] TING WANG,[1,2] XI YANG,[3] MINGYU ZHANG,[3] CHAOJIE PI,[1] JIE YU,[1,4] DACHENG ZHOU,[1] XUE YU,[1] JIANBEI QIU,[1,5] AND XUHUI XU[1,6]

[1]*Faculty of Materials Science and Engineering, Kunming University of Science and Technology, Kunming, 650093, China*
[2]*Department of Applied Physics, The Hong Kong Polytechnic University, NO. 11 Yu Cai Road, Hong Kong, China*
[3]*Yunnan Provincial Energy Research Institute Company Limited, China*
[4]*yujiekmust@163.com*
[5]*qiu@kmust.edu.cn*
[6]*xuxuh07@126.com*

Abstract: Optical performance of the lead halide perovskites with zero-dimension (0D) structure has been in a hot debate for optoelectronic applications. Here, Cs_4PbBr_6 hexagonal micro-particles with a remarkable green emission are first fabricated via a low-temperature solution-process employed ethanol as solvent. Our results underline that the existence of bromine vacancies and the introduction of hydroxyl induce a narrowed band gap with the formation of a defect level, which contributes to the extrinsic photoluminescence (PL) properties synergistically. Thanks to the high exciton binding energy and the unique morphology with a regular geometric structure of the as-obtained micro-particles, two-photon pumped amplified spontaneous emission (ASE) and single mode lasing from an individual Cs_4PbBr_6 particle are realized. Our results not only provide an insight into the origin of optical emission from Cs_4PbBr_6, but also demonstrate that the versatile Cs_4PbBr_6 offers a new opportunity for novel nonlinear photonics applications as an up-conversion laser.

© 2019 Optical Society of America under the terms of the OSA Open Access Publishing Agreement

1. Introduction

Unlike three-dimension (3D) structure perovskites [1–4], in zero-dimension (0D) structure perovskite Cs_4PbBr_6, the $[PbBr_6]^{4-}$ octahedra are isolated from each other and surrounded by Cs^+ cations, resulting in strong quantum confinement and strong exciton-phonon interactions (≥170 meV) [5,6]. Thus, these 0D perovskites represent ideal platforms for fundamental photo-physical studies of polarons, excitons and charge carriers.

Osman M. Bakr advocated the remarkable green intrinsic emission properties from Cs_4PbBr_6 for the first time [6], and then Zhang et al. further demonstrated a high photoluminescence (PL) quantum yield (QY) (~65%) of Cs_4PbBr_6 nanocrystals (NCs) [7]. Afterwards, PL images of Cs_4PbBr_6 microdisks and single crystals confirmed the intrinsic PL emissions come from these 0D structure perovskite Cs_4PbBr_6 [8,9].

Even through extensive studies have been made on the PL of 0D perovskite within recent years, the exact original mechanism of the green emission is still being discussed controversially. Notably, non-luminescent Cs_4PbBr_6 NCs have been explored and a transformation of non-luminescent Cs_4PbBr_6 to highly luminescent $CsPbBr_3$ as well as a decomposition of $CsPbBr_3$ into non-emissive Cs_4PbBr_6 has been demonstrated [10,11]. More specific, no particular crystalline phase due to the identical electron diffraction patterns of emissive Cs_4PbX_6 (X = Cl,

#370873 https://doi.org/10.1364/OE.27.031207
Journal © 2019 Received 3 Jul 2019; revised 5 Sep 2019; accepted 21 Sep 2019; published 14 Oct 2019

Optics EXPRESS

Br, I) and non-emissive Cs_4PbX_6 making the PL origin even more intriguing. Chen et al. reported the bright green emission of Cs_4PbBr_6 is originated from exciton recombination confined in $[PbBr_6]^{4-}$ octahedra [12]. However, the majority of studies agree that Cs_4PbBr_6 have a large bandgap (>3.2 eV), such a high band-gap material cannot show PL in the visible regions for band to band pure exciton transitions [13–16]. An impurity phase of $CsPbBr_3$ in Cs_4PbBr_6 crystals is believed to be the occurrence of green luminescence [17]. Nonetheless, Mohammed and Bakr group ascribed the origin of the PL to the presence of intrinsic defects, such as bromide vacancies, via synthesizing Cs_4PbBr_6 single crystals to rule out the morphological defects of $CsPbBr_3$ [18]. Thus, a plausible interpretation for the origin of the PL is the presence of shallow or deep energy defects with the formation of sub-bandgap states whose energies are related to the formation energy of the defect itself. Among the possible types of defects, the most prevalent defects are halogen vacancies, which behave as radiative recombination centers by forming sub-bandgap states where excitons get trapped [19–22].

Moreover, Zhang et al. described those emissive Cs_4PbBr_6 phases, including powers and NCs, were generated in the presence of a polar solvent (i.e., dimethylformamide) [7], whereas those non-emissive phases were synthesized in an environment of nonpolar solvent (i.e., octadecene) [14]. Notably, although polar solvents like water give rise to chemical instability of perovskites [23,24], water [25] molecules improve the quality of perovskite films and promote the device performance reversibly have also been reported [26]. Wenke Zhou et al. believed the hydrogen bonding between the hydroxyl in water and the iodide ion in perovskite induced the deactivation process, changing the deep defect states to shallow ones [27]. Therefore, some problematic advantages of hydroxyl would not be possible overlooked during the PL process of 0D perovskite.

Herein, the stable 0D Cs_4PbBr_6 micro-particles with "defect" structures were synthesized by a simple polar solution-based method employed ethyl alcohol as solution for the first time. The origin of the intriguing PL is clarified in details by using experimental analysis and theoretical calculation, which verifies the introduction of hydroxyl induces the PL process with the assistant of Br vacancies. In addition, an amplified spontaneous emission (ASE) and a single-mode lasing from an individual Cs_4PbBr_6 micro-particle is readily achieved with the excitation of 800 nm femtosecond (fs) laser. All these results evidently suggest that stable Cs_4PbBr_6 micro-particles provide a promising application for integrated photonic devices.

2. Experimental

Cesium (I) bromide (CsBr, Sigma-Aldrich), lead (II) bromide ($PbBr_2$, Sigma-Aldrich), and dimethyl sulfoxide (DMSO) were used without further purification. The precursor solution was prepared by dissolving 0.05 M CsBr, 0.2 M $PbBr_2$ in 10 mL DMSO. The as-obtained solution was magnetic stirring for 12 h, and 0.9 mL of HBr was added afterward and stirred for 0.5 h for fully dissolved. The mixed solution was then filtered by using an injection filter. Simple drop-immersion of ethanol with a dosage of 200 μL was employed in the obtained filtrate until 3 mL ethanol was added. The yellow precipitate was finally obtained after the solution became limpidity from an appreciably turbid condition following the addition of 3 mL ethanol. After centrifuged with 3 min, the limpidity solution was washed with acetone and centrifuged to obtain the deposition, and then the final powder was collected after drying in a vacuum oven for 24 h. The experimental process is described in Fig. 1.

The powder X-ray diffraction (XRD) patterns were collected using a Bruker AXS D8 diffractometer. The microstructures were recorded by transmission electron microscopy (TEM) and high-resolution field transmission electron microscopy (HRTEM) using U.S. FEI TecnaiG2 F20 operating at 200 kV. The absorption spectra were measured on a HITACHI U-4100 type spectrophotometer (Hitachi, Tokyo, Japan). The photo-luminescence excitation (PLE) and PL spectra were recorded by a HITACHI-F-7000 spectrophotometer. For the lasing measurement, a homemade micro-PL system (OlympusBX-52 microscope and a 20×0.8 NA objective lens)

Optics EXPRESS

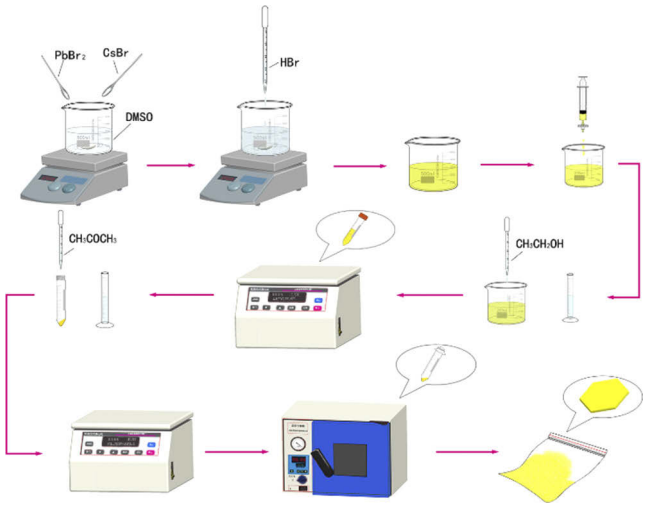

Fig. 1. Scheme Illustration of the preparation process.

was used to focus 800 nm femtosecond laser beam to be a 5 μm diameter spot at different area of microplates. A Ti: sapphire femtosecond laser (Coherent Libra) integrated with an optical parametric amplifier (Coherent OPerA Solo), which generated femtosecond pulses (50 fs,1 kHz) was used as the excitation source. Cs_4PbBr_6 hexagonal micro-particles located inside the low-temperature (77 K) chamber was excited by the laser spot. Emission observed from the microcavity was then collected by the same objective lens. The received optical signal emitted from the microcavity was either coupled to a conventional charge-coupled device (CCD) camera for the recording of the near-field image or attached to a monochromator (Princeton SpectraPro 2750 integrated with a ProEM EMCCD camera with spectral resolution less than 0.1 nm) for spectrum analysis. Fourier transform infrared (FT-IR) spectra were measured by a Nicolet is 10 Fourier transform infrared spectrometer. The chemical states of Cs_4PbBr_6 micro-particles were characterized by X-ray photoelectron spectroscopy (XPS) (200 W) with Al Kα radiation under the vacuum conditions. The first principles calculations were performed by the planewave pseudopotential method implemented in the CASTEP package based on the density functional theory (DFT) calculations [28]. The ion-electron interactions were modeled by ultrasoft pseudopotentials [29] for all elements. The generalized gradient approximation (GGA) [30] was adopted to describe the exchange and correlation potentials. The kinetic energy cutoff of 380 eV and Monkhorst-Pack k-point meshes [31] with a density of (3×3×3) points in the Brillouin zone were chosen.

3. Results and discussion

The XRD patterns of the sample indicate that the perovskite structure is formed (Fig. 2(a)), in which a series of diffraction peaks can be indexed to the planes of hexagonal space group $R\bar{3}c$ of perovskite structure (JCPDS No.73-2478) [7]. SEM characterizations (Fig. 2(b)) confirm that the as-obtained yellow samples are micro-meter sized particles with an average particle size of ~ 30 μm. The mapping images of the particles demonstrate the well dispersion of elements of Cs, Pb and Br in the as-obtained Cs_4PbBr_6 particles as exhibited in Fig. 2(c). A strong green emission located at 538 nm is recorded under 310 nm excitation, and the photograph of the green emission originated from an individual particle is presented in the inset of Fig. 2(d). The observed green emission is believed to be derived from individual Cs_4PbBr_6 particle rather than $CsPbBr_3$. It should be pointed out that a sharp absorption (310 nm) is observed, along with a strong absorption

Optics EXPRESS

edgy appears around 514 nm in the absorption spectrum as shown in Fig. 2(d). This result infers that the two absorption band corresponds to the band gap absorption of Cs_4PbBr_6 and a mid-band gap related to the introduction of defect level.

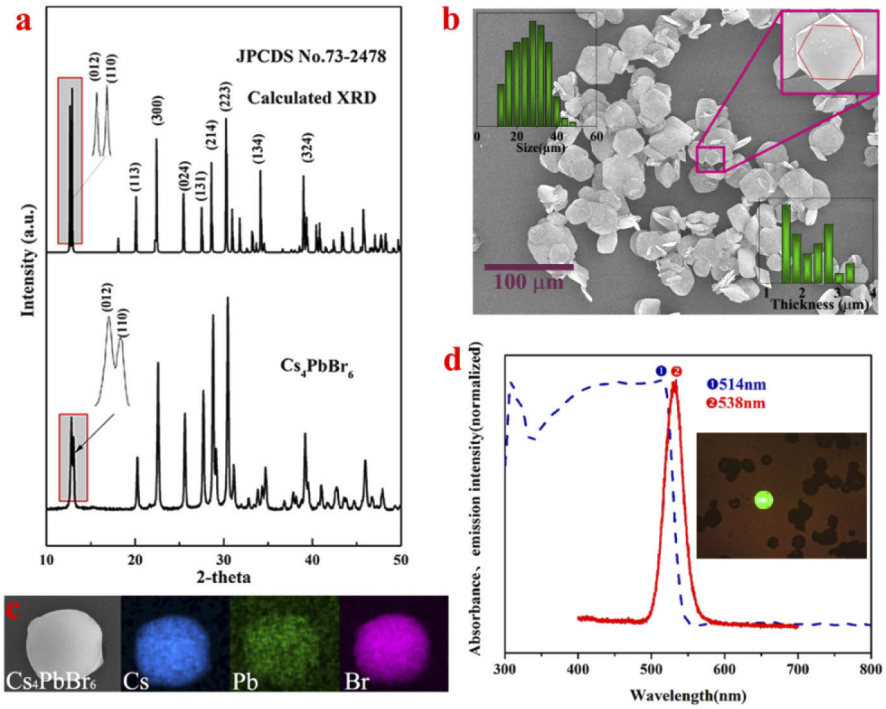

Fig. 2. (a) The calculated XRD patterns of Cs_4PbBr_6 and the experimental XRD patterns. (b) SEM and (c) element mapping images of the as-obtained Cs_4PbBr_6 with a mean size of 30 μm and a thickness less than 3.4 μm, (the inset in the upper right corner of Fig. 1(b) exhibits the morphology of a single particle and the histogram of the inset describes the size and thickness distribution of the as-obtained Cs_4PbBr_6 particles). (d) PL and absorption spectra of Cs_4PbBr_6 particles (the inset of Fig. 2(d) shows the bright green emission from a single particle).

The FT-IR spectrum illustrates that a broad peak of hydroxide (-OH) appears in the synthesized Cs_4PbBr_6 via the polar solution-based synthesis method, compared with its counterpart synthesized via a hot-injection process [32] (Fig. 3(a)). Moreover, the XPS spectrum displays the co-existence of Pb-Br bonds and Pb-O bonds (Fig. 3(b)), further demonstrating that the fabricated microcrystals contain a mass of bromine vacancies, some of which would be occupied by -OH to form Pb-O bond. The band structure and density of states properties of the 0D perovskite is investigated by the first-principles calculations. Cs_4PbBr_6 has a bandgap with 3.76 eV (Fig. 3(c)) which is consistent with the results reported by Manna et al. [14], so the absorption at around 310 nm corresponds to the band gap for the GGA calculation underestimates the band gap in some extent. As shown in Fig. 3(c), the valence band (VB) is mainly formed by the p orbitals of bromine, and conduction band (CB) is made up of Pb-p orbitals with a little Br-s and Br-p orbitals, which means $[PbBr_6]^{4-}$ octahedra dictate the optical transition behavior of perovskite materials. It should be pointed out that pure Cs_4PbBr_6 with an energy gap of 3.76 eV should not exhibit PL at 550 nm for a interband transition. Thus, the green emission is possible only when defects are introduced to the band gap [18]. Moreover, although it is concluded that high V_{Br} concentrations result in a lower radiative recombination efficiency, and a consequent decrease in PLQY, the

Optics EXPRESS

recombination from mid-bandgap states due to crystal defects is identified as being the origin of the green PL in Cs_4PbBr_6 [33]. The existence of a bromide vacancy introduce a sub-bandgap state 2.75 eV located in Cs_4PbBr_6 as shown in Fig. 3(d). Unfortunately, the existence of bromide vacancy bring the green emission seems illogical. The incorporation of -OH groups as a defect is considerate to be introduced into Cs_4PbBr_6 [34], however, through DFT calculations, the bandgap decreases with the introduction of -OH, the bandgap decreases from 3.75 to 3.50 eV (Fig. 3(e)) without the presence of the sub-bandgap state. This result is inconsistent with the report which proposed the incorporation of -OH groups form a 2.6 eV sub-bandgap state in Cs_4PbBr_6 [35]. Furthermore, it is found that the incorporation of -OH and bromide vacancies contributes to a sub-bandgap at 2.44 eV in Cs_4PbBr_6 with a narrowed energy gap (3.50 eV) (Fig. 3(f)). It is revealed that bromide vacancies are the dominant defects that responsible for the intrinsic n-type conduction in Cs_4PbBr_6, while the introduction of -OH contributes to the decrease of the band-gap, the synergistic effect of which induces the quite unambiguously green emission. The above results demonstrate the introduction of bromine vacancies and hydroxyl groups, contribute to the extrinsic luminescence properties synergistically.

In general, trap state density as a key factor seriously deteriorates the stimulated emission properties by causing the loss of photon-generated carriers through fast nonradiative recombination [36]. However, what unexpected in this work is that Cs_4PbBr_6 micro-particles with "defect" structures of bromine vacancies and hydroxyl groups exhibit excellent stimulated emission properties under two-photon pumping by using Ti: sapphire laser system from Coherent (800 nm, 45 fs, 1 kHz repetition rate). During the lasing measurement, we perform a confocal micro-photoluminescence spectrometer to detect the PL spectra of a single particle (see Figs. 4(c) and 5(c)). When the pump light source is focused at the edge of the particle, the intensity of the green emission increases with increasing pump power, and subsequently a bright green emission can be observed with naked eyes, as shown in Figs. 4(a) and 4(b). Figure 4(d) plots the total PL intensity and full width at half-maximum (FWHM) under different excitation density of Cs_4PbBr_6 micro-particles. Under 800 nm pumping with a low excitation density (<125.00 $\mu J/cm^2$), the emission intensity of Cs_4PbBr_6 micro-particles follow a quadratic dependence on the pump power with a slope K ($K = \log I_{PL}/\log I_{exc}$) of ~1.62 [37], suggesting the domination of the two-photon absorption mechanism. When the excitation density increases above 125.00 $\mu J/cm^2$, the PL intensity is drastically increased with the excitation density, which presents a non-linear dependence of the PL intensity on the pumping energy. Concerning the FWHM (Fig. 4(d)), a clear line narrowing, from 12.6 nm down to about 3.2 nm as the excitation density increases is observed. The strong PL intensity increases and the line narrowing occur with the increase of excitation density, ambiguously demonstrating the appearance of ASE phenomenon. For the unique morphology of our obtained particles as shown in Fig. 4(c), it is hard to achieve a cavity for supporting laser loop feedback for excited from the edge of the micro-particle because of the non-parallel geometry.

For the unique morphology of our obtained particles which has a parallel upper and lower surface at the center of the particle and unparalleled surface around the edge of the particle, the PL spectra of these macro-particles were recorded for the pump light source focused at the center of the particle as presented in Figs. 5(a) and 5(b). A bright green emission and optical waveguide phenomenon is observed under 800 nm fs pumping as well. Moreover, it can be seen that a single sharp peak abruptly appears above the spontaneous emission background and grows drastically with further increasing pump density. Importantly, no other resonant peaks were found during this process. The corresponding changes of the integrated emission intensity and FWHM as a function of pump intensity are plotted in Fig. 5(d). When the pumping power increases over 153.5 $\mu J/cm^2$, a very sharp lasing peak centered at 538 nm in combination with a sharp decrease in FWHM to 0.4 nm emerges, and the lasing intensity grows rapidly with the increase of pump intensity. A clear evolvement from above optical characteristics indicates the achievement of a

Optics EXPRESS

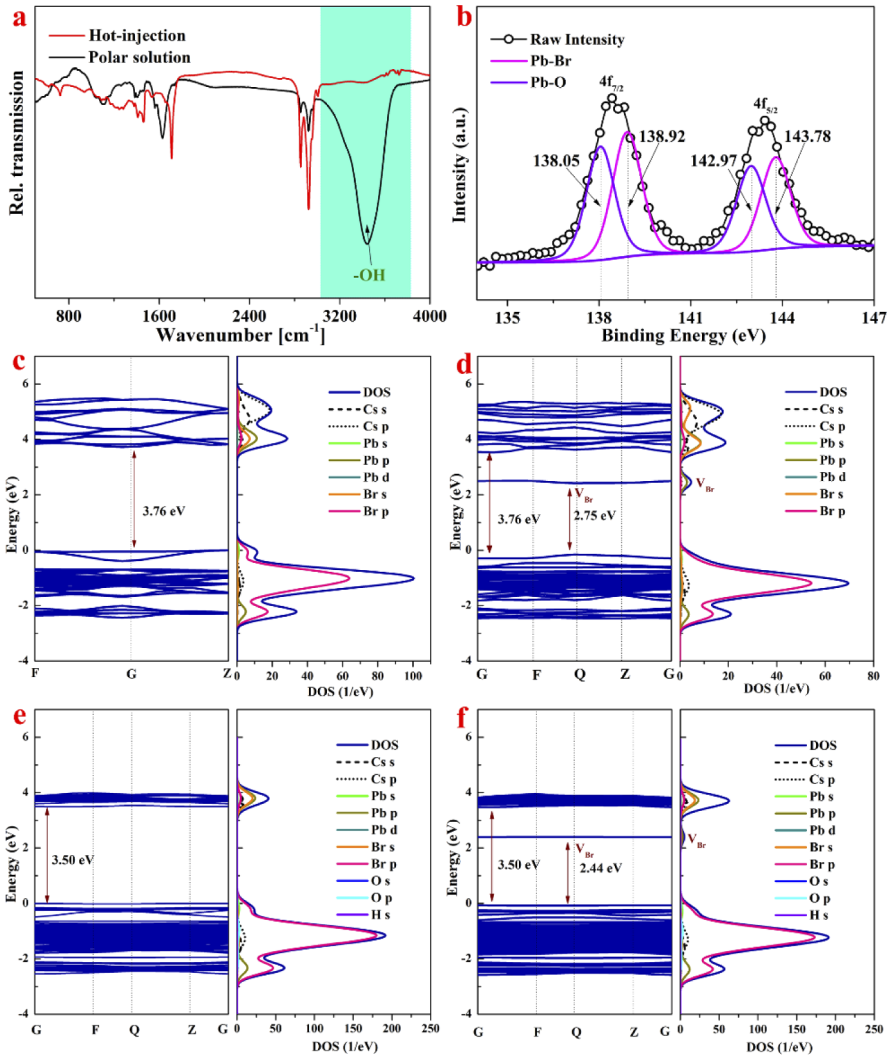

Fig. 3. (a) FT-IR spectra of the Cs_4PbBr_6 micro-particles obtained via the hot-injection and the polar solution-based synthesis method, respectively. (b) XPS spectrum of Pb 4f in Cs_4PbBr_6 micro-particles synthesized via the polar solution-based synthesis method, and the XPS spectrum were calibrated using C1s peak at 284.8 eV. Band structure and density of state of (c) Cs_4PbBr_6; (d) Cs_4PbBr_6+V_{Br}; (e) Cs_4PbBr_6+OH; and (f) Cs_4PbBr_6+V_{Br} +OH, respectively.

Optics EXPRESS

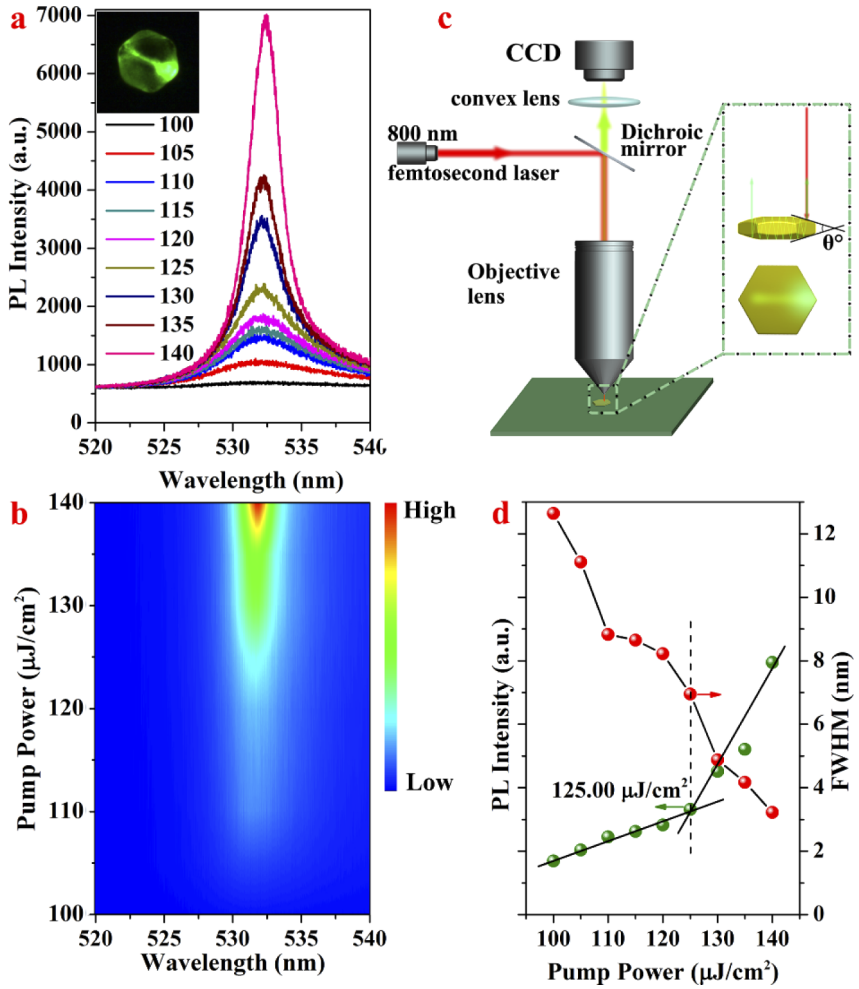

Fig. 4. (a) PL spectra and (b) the corresponding PL mapping versus pumping density at room temperature under 800 nm laser, and the inset in Fig. 4(a) is the photograph of an individual hexagonal particle under 800 nm femtosecond laser pumping from the edge of the particle. (c) Schematic description of the Cs_4PbBr_6 micro-particle under 800 nm femtosecond laser excitation. (d) The dependence of the PL intensity and FWHM as a function of pumping density under 800 nm femtosecond laser excitation.

Optics EXPRESS

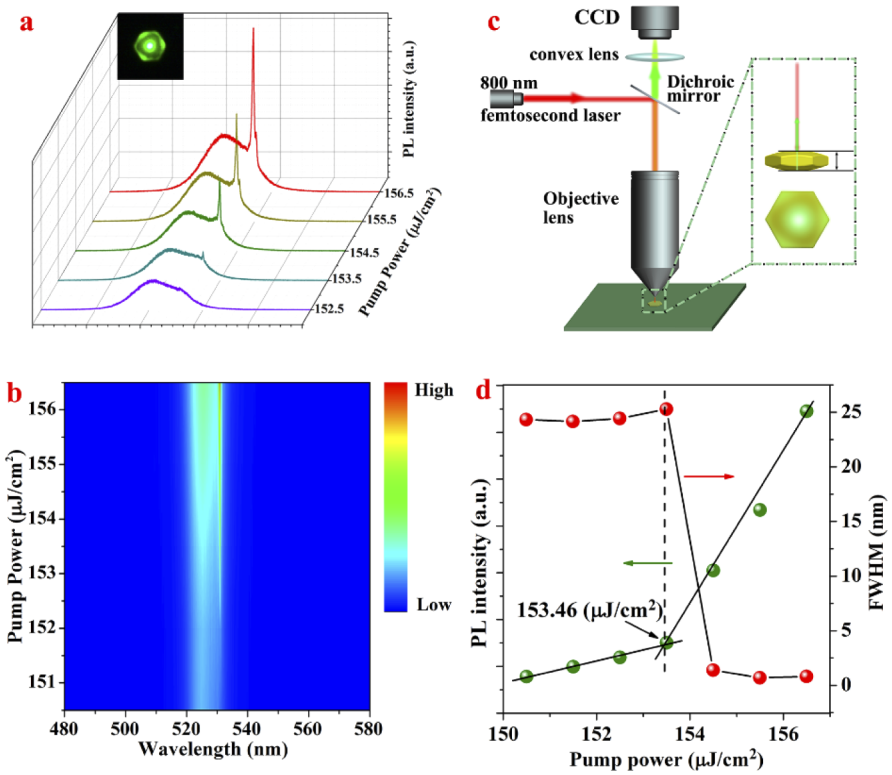

Fig. 5. (a) Lasing spectra and (b) the corresponding lasing spectra mapping from a single Cs_4PbBr_6 micro-particle around the lasing threshold, and the inset in Fig. 5(a) is the photograph of an individual hexagonal particle under 800 nm femtosecond laser pumping focused on the center region of the particle. (c) Schematic description of the Cs_4PbBr_6 micro-particle under 800 nm femtosecond laser excitation focused on the center region of the particle. (d) The dependence of the output intensity and linewidth as a function of pumping density under 800 nm femtosecond laser excitation, showing the threshold of around 153 μJ cm^{-2}.

single-mode laser. Single-mode lasing achieved from a particle if the free spectral range of the cavity is larger than the band-width of the gain material, and the latter is evaluated to be 3.2 nm from the FWHM of the ASE spectra of single particle. Here, we estimate the mode spacing, $\Delta\lambda$, of plate microcavity [37],

$$\Delta\lambda = \lambda^2/(2n_gL) \tag{1}$$

where λ is the center of the emission wavelength, n_g is the group refractive index of ≈3.7 and 2L is the cavity length of microcrystal. $\Delta\lambda$ is estimated to be 11.5 nm for a Fabry-perot cavity provided with the particle for the thickness of 3.4 μm, which is clearly larger than the gain bandwidth value. Therefore, a single mode lasing could be realized for a natural feedback cavity for the F-P laser model with the micro-particles, when the excitation focused on the parallel symmetry of the upper and lower surface of our particle. In fact, the WGM mode is excluded for the absence of the observation of the excited light around the edge of Cs_4PbBr_6 micro-particle. Moreover, $\Delta\lambda$ is calculated to be 1.6 nm when the cavity length is 48.56 μm of the micro-particle for a WGM mode, which indicates that a multi rather than single mode lasing should appear, inconsistent with our observation. Thus, a single mode F-P lasing output could be readily achieved in this

Optics EXPRESS

work thanks to the laser loop feedback provided with the macro-particles for the thickness below 3.4 μm.

4. Conclusion

In summary, Cs_4PbBr_6 micro-particles, which possess a 0D perovskite structure, are first fabricated via a low-temperature solution-process employed ethanol as solvent. Fluorescence image studies down to the single-particle level confirm the PL of bright green emission from an individual particle. Our results underline that the introduction of hydroxyl and the existence of bromine vacancies results in a narrowed band gap with the formation of a defect level, which contributes to the extrinsic PL properties synergistically. Because of the high exciton binding energy and the unique morphology with a regular geometric structure, two-photon pumped ASE and a single-mode lasing based on an individual Cs_4PbBr_6 micro-particle are readily achieved by an 800 nm femtosecond laser. These results suggest that 0D perovskite Cs_4PbBr_6 with "defect" structures could be promising candidates for the future development of perovskite materials based light-emitting diodes and lasers.

Funding

National Natural Science Foundation of China (11664022, 61965012); the Reserve talents project of Yunnan Province (2017HB011); Yunnan Ten Thousand Talents Plan Young & Elite Talents Project (YNWR-QNBJ-2018-295, YNWR-QNBJ-2018-325).

References

1. X. Du, G. Wu, J. Cheng, H. Dang, K. Ma, Y. W. Zhang, P. F. Tan, and S. Chen, "High-quality $CsPbBr_3$ perovskite nanocrystals for quantum dot light-emitting diodes," RSC Adv. **7**(17), 10391–10396 (2017).
2. E. L. Unger, L. Kegelmann, K. Suchan, D. Sörell, L. Korte, and S. Albrecht, "Roadmap and roadblocks for the band gap tunability of metal halide perovskites," J. Mater. Chem. A **5**(23), 11401–11409 (2017).
3. M. Abdi-Jalebi, M. Ibrahim Dar, S. P. Senanayak, A. Sadhanala, Z. Andaji-Garmaroudi, L. M. Pazos-Outón, J. M. Richter, A. J. Pearson, H. Sirringhaus, M. Grätzel, and R. H. Friend, "Charge extraction via graded doping of hole transport layers gives highly luminescent and stable metal halide perovskite devices," Sci. Adv. **5**(2), eaav2012 (2019).
4. M. Wei, F. P. G. de Arquer, G. Walters, Z. Yang, L. N. Quan, Y. Kim, R. Sabatini, R. Quintero-Bermudez, L. Gao, J. Z. Fan, F. Fan, A. Gold-Parker, M. F. Toney, and E. H. Sargent, "Ultrafast narrowband exciton routing within layered perovskite nanoplatelets enables low-loss luminescent solar concentrators," Nat. Energy **4**(3), 197–205 (2019).
5. J. W. Choi, N. Cho, H. C. Woo, B. M. Oh, J. Almutlaq, O. M. Bakr, S.-H. Kim, C.-L. Lee, and J. H. Kim, "Investigation of high contrast and reversible luminescence thermochromism of the quantum confined Cs_4PbBr_6 perovskite solid," Nanoscale **11**(12), 5754–5759 (2019).
6. J. Yin, Y. Zhang, A. Bruno, C. Soci, O. M. Bakr, J.-L. Brédas, and O. F. Mohammed, "Intrinsic Lead Ion Emissions in Zero-Dimensional Cs_4PbBr_6 Nanocrystals," ACS Energy Lett. **2**(12), 2805–2811 (2017).
7. Y. Zhang, M. I. Saidaminov, I. Dursun, H. Yang, B. Murali, E. Alarousu, E. Yengel, B. A. Alshankiti, O. M. Bakr, and O. F. Mohammed, "Zero-Dimensional Cs_4PbBr_6 Perovskite Nanocrystals," J. Phys. Chem. Lett. **8**(5), 961–965 (2017).
8. Q. Luo, H. Wang, X. Yin, and L. Wang, "Hydrophilic perovskite microdisks with excellent stability and strong fluorescence for recyclable temperature sensing," Sci. China Mater. **62**(7), 1065–1070 (2019).
9. J. H. Cha, J. H. Han, W. Yin, C. Park, Y. Park, T. K. Ahn, J. H. Cho, and D. Y. Jung, "Photoresponse of $CsPbBr_3$ and Cs_4PbBr_6 Perovskite Single Crystals," J. Phys. Chem. Lett. **8**(3), 565–570 (2017).
10. L. Rao, X. Ding, X. Du, G. Liang, Y. Tang, K. Tang, and J. Z. Zhang, "Ultrasonication-assisted synthesis of $CsPbBr_3$ and Cs_4PbBr_6 perovskite nanocrystals and their reversible transformation," Beilstein J. Nanotechnol. **10**(1), 666–676 (2019).
11. Y. Li, H. Huang, Y. Xiong, S. V. Kershaw, and A. L. Rogach, "Reversible transformation between $CsPbBr_3$ and Cs_4PbBr_6 nanocrystals," CrystEngComm **20**(34), 4900–4904 (2018).
12. D. Chen, Z. Wan, X. Chen, Y. Yuan, and J. Zhong, "Large-scale room-temperature synthesis and optical properties of perovskite-related Cs_4PbBr_6 fluorophores," J. Mater. Chem. C **4**(45), 10646–10653 (2016).
13. Z. Zhang, Y. Zhu, W. Wang, W. Zheng, R. Lin, X. Li, H. Zhang, D. Zhong, and F. Huang, "Aqueous Solution Growth of Millimeter-Sized Nongreen-Luminescent Wide Bandgap Cs_4PbBr_6 Bulk Crystal," Cryst. Growth Des. **18**(11), 6393–6398 (2018).

Optics EXPRESS

14. Q. A. Akkerman, S. Park, E. Radicchi, F. Nunzi, E. Mosconi, F. De Angelis, R. Brescia, P. Rastogi, M. Prato, and L. Manna, "Nearly Monodisperse Insulator Cs_4PbX_6 (X = Cl, Br, I) Nanocrystals, Their Mixed Halide Compositions, and Their Transformation into $CsPbX_3$ Nanocrystals," Nano Lett. **17**(3), 1924–1930 (2017).
15. M. De Bastiani, I. Dursun, Y. Zhang, B. A. Alshankiti, X.-H. Miao, J. Yin, E. Yengel, E. Alarousu, B. Turedi, J. M. Almutlaq, M. I. Saidaminov, S. Mitra, I. Gereige, A. AlSaggaf, Y. Zhu, Y. Han, I. S. Roqan, J.-L. Bredas, O. F. Mohammed, and O. M. Bakr, "Inside Perovskites: Quantum Luminescence from Bulk Cs_4PbBr_6 Single Crystals," Chem. Mater. **29**(17), 7108–7113 (2017).
16. D. Wang, W.-B. Shi, H. Jing, C. Yin, Y. Zhu, J. Su, G.-B. Ma, R. Peng, X. Wang, and M. Wang, "Photon-induced carrier recombination in the nonlayered-structured hybrid organicinorganic perovskite nano-sheets," Opt. Express **26**(21), 27504–27514 (2018).
17. Y. Wang, D. Yu, Z. Wang, X. Li, X. Chen, V. Nalla, H. Zeng, and H. Sun, "Solution-Grown $CsPbBr_3/Cs_4PbBr_6$ Perovskite Nanocomposites: Toward Temperature-Insensitive Optical Gain," Small **13**(34), 1701587 (2017).
18. J. Yin, H. Yang, K. Song, A. M. El-Zohry, Y. Han, O. M. Bakr, J.-L. Brédas, and O. F. Mohammed, "Point Defects and Green Emission in Zero-Dimensional Perovskites," J. Phys. Chem. Lett. **9**(18), 5490–5495 (2018).
19. S. Seth, N. Mondal, S. Patra, and A. Samanta, "Fluorescence Blinking and Photoactivation of All-Inorganic Perovskite Nanocrystals $CsPbBr_3$ and $CsPbBr_2I$," J. Phys. Chem. Lett. **7**(2), 266–271 (2016).
20. J. M. Ball and A. Petrozza, "Defects in perovskite-halides and their effects in solar cells," Nat. Energy **1**(11), 16149 (2016).
21. J. Kang and L.-W. Wang, "High Defect Tolerance in Lead Halide Perovskite $CsPbBr_3$," J. Phys. Chem. Lett. **8**(2), 489–493 (2017).
22. S. Seth and A. Samanta, "Fluorescent Phase-Pure Zero-Dimensional Perovskite-Related Cs_4PbBr_6 Microdisks: Synthesis and Single-Particle Imaging Study," J. Phys. Chem. Lett. **8**(18), 4461–4467 (2017).
23. L. N. Quan, M. Yuan, R. Comin, O. Voznyy, E. M. Beauregard, S. Hoogland, A. Buin, A. R. Kirmani, K. Zhao, A. Amassian, D. H. Kim, and E. H. Sargent, "Ligand-Stabilized Reduced-Dimensionality Perovskites," J. Am. Chem. Soc. **138**(8), 2649–2655 (2016).
24. Y. Fang, H. Wei, Q. Dong, and J. Huang, "Quantification of re-absorption and re-emission processes to determine photon recycling efficiency in perovskite single crystals," Nat. Commun. **8**(1), 14417 (2017).
25. B. Turedi, K. J. Lee, I. Dursun, B. Alamer, Z. Wu, E. Alarousu, O. F. Mohammed, N. Cho, and O. M. Bakr, "Water-induced dimensionality reduction in metal-halide perovskites," J. Phys. Chem. C **122**(25), 14128–14134 (2018).
26. X. Gong, M. Li, X.-B. Shi, H. Ma, Z.-K. Wang, and L.-S. Liao, "Controllable Perovskite Crystallization by Water Additive for High-Performance Solar Cells," Adv. Funct. Mater. **25**(42), 6671–6678 (2015).
27. W. Zhou, Y. Zhao, C. Shi, H. Huang, J. Wei, R. Fu, K. Liu, D. Yu, and Q. Zhao, "Reversible Healing Effect of Water Molecules on Fully Crystallized Metal–Halide Perovskite Film," J. Mater. Chem. C **120**(9), 4759–4765 (2016).
28. S. J. Clark, M. D. Segall, C. J. Pickard, P. J. Hasnip, M. I. Probert, K. Refson, and M. C. Payne, "First principles methods using CASTEP," Z. Kristallogr. - Cryst. Mater. **220**(5/6), 567–570 (2005).
29. D. Vanderbilt, "Soft self-consistent pseudopotentials in a generalized eigenvalue formalism," Phys. Rev. B **41**(11), 7892–7895 (1990).
30. J. P. Perdew, K. Burke, and K. M. Ernzerhof, "Generalized Gradient Approximation Made Simple," Phys. Rev. Lett. **77**(18), 3865–3868 (1996).
31. H. J. Monkhorst and J. D. Pack, "Special points for Brillouin-zone integrations," Phys. Rev. B **13**(12), 5188–5192 (1976).
32. L. Wu, H. Hu, Y. Xu, S. Jiang, M. Chen, Q. Zhong, D. Yang, Q. Liu, Y. Zhao, B. Sun, Q. Zhang, and Y. Yin, "From Nonluminescent Cs_4PbX_6 (X = Cl, Br, I) Nanocrystals to Highly Luminescent $CsPbX_3$ Nanocrystals: Water-Triggered Transformation through a CsX-Stripping Mechanism," Nano Lett. **17**(9), 5799–5804 (2017).
33. B. Kang and K. Biswas, "Exploring Polaronic, Excitonic Structures and Luminescence in $Cs_4PbBr_6/CsPbBr_3$," J. Phys. Chem. Lett. **9**(4), 830–836 (2018).
34. N. Riesen, M. Lockrey, K. Badek, and H. Riesen, "On the origins of the green luminescence in the "zero-dimensional perovskite" Cs_4PbBr_6: conclusive results from cathodoluminescence imaging," Nanoscale **11**(9), 3925–3932 (2019).
35. Q. A. Akkerman, A. L. Abdelhady, and L. Manna, "Zero-Dimensional Cesium Lead Halides: History, Properties, and Challenges," J. Phys. Chem. Lett. **9**(9), 2326–2337 (2018).
36. S. Chen, X. Wen, S. Huang, F. Huang, Y.-B. Cheng, M. Green, and A. Ho-Baillie, "Light Illumination Induced Photoluminescence Enhancement and Quenching in Lead Halide Perovskite," Sol. RRL **1**(1), 1600001 (2017).
37. B. Zhou, M. Jiang, H. Dong, W. Zheng, Y. Huang, J. Han, A. Pan, and L. Zhang, "High-Temperature Upconverted Single-Mode Lasing in 3D Fully Inorganic Perovskite Microcubic Cavity," ACS Photonics **6**(3), 793–801 (2019).

158.132.161.52 {ts '2020-01-22 02:32:27'}